# The Dynamic Mechanical Behaviour and the Statistical Crack Mechanics Model for a Polymer-bonded Explosive

**L. CHENG[1], H. SHI[1], R. CHEN[2,*], F. LU[2]**
[1] Tsinghua University, School of Aerospace, AML, Department of Engineering Mechanics,Beijing 100084, P. R. China
[2] National University of Defense Technology, College of Science, Changsha 410073, P. R. China

*Polymer-bonded explosives (PBXs) are widely used in various engineering applications. Thus, the safety of PBXs has received much attention. In this study, dynamic experiments on a typical PBX were conducted and the mechanical behaviour was studied. Based on the statistical crack mechanics (SCRAM) model, two constitutive models, the Visco-SCRAM model and the Elastic-Plastic-SCRAM model, were developed. Finite element simulations have also been carried out by applying the Visco-SCRAM model and the Elastic-Plastic-SCRAM model in the simulations and good agreement was found between the simulation results and the experimental results. It is suggested that the Elastic-Plastic-SCRAM model can be used for simulating the dynamic behaviour of PBXs under high strain rate conditions.*

*Keywords: PBXs; Elastic-Plastic-SCRAM model; Visco-SCRAM model*

After some terrible disasters about energetic materials, clearly, less sensitive monition is in need to avoid these kinds of accidents in the future. Therefore, accurately predicting the failure and non-shock ignition responses of PBXs is critical. Until recently, researchers studying energetic materials have developed many investigations on the non-shock ignition responses of PBXs through experimentations and simulations [1].

Current studies on the safety of energetic materials are mainly concentrated on their relevant mechanical properties in relation to loading conditions and application environment, the emphasis of which is their dynamic mechanical properties. A great amount of studies has been carried out on the dynamic compressive mechanical properties. Rangaswamy et al. [2] obtained the compressive and tensile mechanical properties of PBX9501 under different strain rates and temperatures. Blumenthal et al. [3] studied the compression performance of PBX110 and explosives based on HTPB through a series of split Hopkinson pressure bar (SHPB) tests. Rae et al. [4, 5] observed the differences of a PBX's mechanical properties before and after temperature aging by using the digital image cross-correlation. Duncan and Margetson[6] developed a uniaxial nonlinear viscoelastic constitutive model to model solid rocket propellants based on a cumulative damage approach. Luo [7] carried out researches on the dynamic mechanical properties of JOB-9003 explosive. Li et al. [8] reported the stress-strain relations of a PBX under different strain rates through quasi-static and dynamic compression tests.

The constitutive models of brittle materials, such as energetic materials, have also received consideration attentions. A micromechanical material model, the statistical crack mechanics (SCRAM), was developed by Dienes and coworkers [9-12] to model the dynamic mechanical deformation and fragmentation of brittle materials based on micromechanical statistical approach. Because of the physical complex and excessive model constants for SCRAM, the model application is limited and many simple models were developed in recent years. Based on Dienes' SCRAM theory, a simplified, isotropic damage model (Iso-SCRAM) was developed by Addessio and Johnson [13]to study the dynamic responses of brittle materials. It is assumed in the Iso-SCRAM model that the micro cracks are isotropic, and the crack radius distribute exponentially. The number of the physical parameters in the model was reduced to the minimum by making these assumptions. However, as for the PBXs, the viscous effects of binder materials should be considered [14]. To concur this problem, a Visco-SCRAM model was developed by Bennett et al. [15] and applied to study the non-shock ignition and the damage and failure behaviour of explosives. They assumed that the crack growth rate depended on the stress intensity, and the uniaxial stress-strain curves of PBX-9501 were well predicted by implementing the Visco-SCRAM constitutive equations into DYNA3D.

In the present study, stress–strain curves under various strain rates and the fracture parameters of a PBX were obtained experimentally via MTS and SHPB tests (Section 2). The Visco-SCRAM model was introduced in Section 3. Based on the experimental results, a novel Elastic-Plastic-SCRAM model was developed by considering the effects of plasticity and damage of the binder matrix in the equation of state (Section 4). Finally, comparisons between the simulation results based on the Elastic-Plastic-SCRAM model and the experimental results were carried out (Section 5).

## Experimental Study on the PBX Mechanical Properties

*Sample preparation*

PBX with aluminized powder can maintain a higher pressure and long period [16]. The main ingredient of the PBX explosives used in this paper are RDX explosives, and binder. The component and grain size distribution of the PBX are shown in Table 1. The RDX powder is prepared according to the eighth category in GJB296A-95[17]. The size of the specimen is Φ10 mm×20 mm for quasi-static tests, and Φ16 mm×10 mm for high strain rate tests. The PBX specimen was pressed in a steel die at the temperature of 100 °C and the pressure of 100 MPa for 1.5 h. The density of the specimen is 1.8 g/cm$^3$.

* *email: R_Chen@nudt.edu.cn (R.C.); Tel.: +86-731-84573267*

| Component | RDX[17] | | Binder |
|---|---|---|---|
| Content (wt%) | 92% | | 8% |
| Grain size | 45μm | 40~60% | -- |
| | 75μm | 35% | |
| | 150μm | 13.5% | |
| | 300~500μm | 1.5% | |
| Average grain size | 74μm | | -- |

**Table 1**
COMPONENT AND GRAIN SIZE DISTRIBUTION OF THE PBX

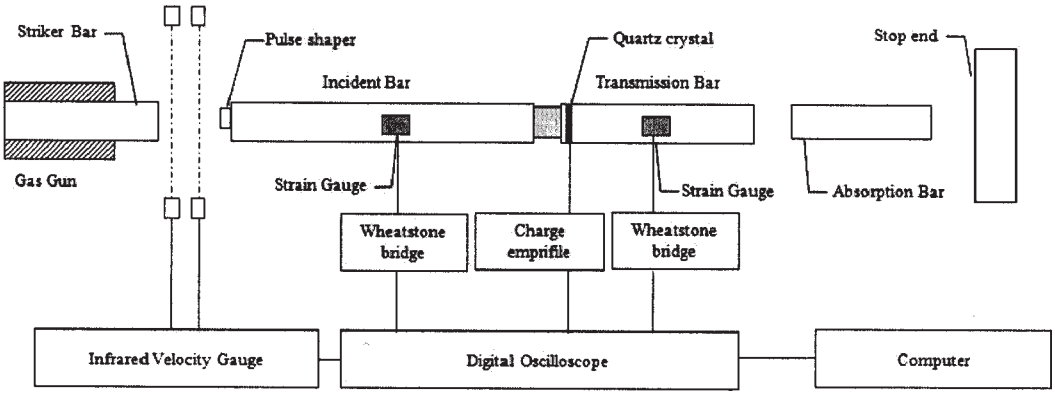


Fig. 1.SHPB and data acquisition systems

*Stress-strain curve measurement*

Quasi-static and high strain rate tests are carried out on the MTS machine and SHPB, respectively. The bars in the SHPB system are 20 mm in diameter (fig. 1) and the striker bar is 150 mm long. The length of the incident bar is 1900 mm and a pair of strain gauges is mounted 1048 mm away from the specimen. The transmission bar has the length of 1100 mm and the strain gauges are mounted 492 mm away from the specimen. The strain gauge on each bar was connected to the opposite arms of a Wheatstone bridge circuits with amplification. As the wave impedance of the PBX is very low and the signal of the transmitted wave is too weak, a pair of piezoelectric transducers was used to measure the loading force directly. The positive pole of the crystal was glued to the bar, and the negative pole was glued to a thin aluminum disk, as shown in figure 1. A charge amplifier was used to collect the quartz crystal signals. The velocity of the striker bar was measured by an infrared system. All the signals are recorded by a four-channel DPO5054 (Tektronix) digital oscilloscope.

The loading force of specimen on the transmitted bar-specimen interface, $F$, is:

$$F = \frac{U_Q}{k_{QC} \cdot k_0} \tag{1}$$

where $k_0$ is the scale factor of the charge amplifier, $U_Q$ is the signal of quartz crystal embedded in the bar, and $k_{QC}$ = $(2.34\pm0.05)\times10^{-12}$C/N is the quartz crystal coefficient[18].

We denote the input, reflected and transmitted strain pulses as $\varepsilon_i(t)$, $\varepsilon_r(t)$, and $\varepsilon_t(t)$, respectively. Thus,

$$\varepsilon_{i,r,t} = \frac{2 \cdot U_{i,r,t}}{k_1 \cdot k_2 \cdot U_0} \tag{2}$$

where $U_{i,r,t}$ is the input, reflected and transmitted signal, respectively. $k_1$ is the scale factor of the pre amplifier, $k_2$ is the strain gauge coefficient and $k_2$=1.97 in the present study.

The pulse shaping technique was also used in the experiments. According to the basic theory of SHPB, we can obtain the strain rate $\dot{\varepsilon}_s(t)$, the strain $\varepsilon_s(t)$, and the stress $\sigma_s(t)$ of the specimen as

$$\dot{\varepsilon}_s(t) = -\frac{2c_0}{l_s}\varepsilon_r(t) \tag{3}$$

$$\varepsilon_s(t) = -\frac{2c_0}{l_s}\int_0 \varepsilon_r(\tau)d\tau \tag{4}$$

$$\sigma_s(t) = \frac{EA_0}{A_s}\varepsilon_t(t) \tag{5}$$

where $E$ is the bar's elastic modulus, $c_0$ is the one-dimensional longitudinal stress wave velocity propagated along the bar, $A_0$ is the sectional area of the bar, $l_0$ and $A_s$ are the length and the cross area of the specimen.

There are two hypotheses required by this technique, one is one-dimensional stress wave propagation in the bars, and the other is stress balance in the specimen for a uniform deformation. As discussed before, brass is adopted widely as a pulse shaper material in SHPB[8,19].A constant strain rate can be achieved using a brass pulse shaper with certain diameter and length. The 2mm-thick brass cylinders with variety diameters were adopted as the pulse shaper in the SHPB tests. The reflected pulse has a plateau stage before failure, as can be seen from figure 2, which represents a constant strain rate loading during the test. Figure 2 shows the oscilloscope signals for a typical test. The signals from the quartz crystal can enhance the magnitude of the transmitted signal by four times, and the signal-to-noise ratio can also be increased obviously. Figure 3 shows the loading histories on both ends of the specimen for a typical test. The dynamic stress on the left side of the specimen is calculated by adding the incident stress and reflected stress waves together (In+Re), and the one on the right side is calculated by the transmitted stress wave

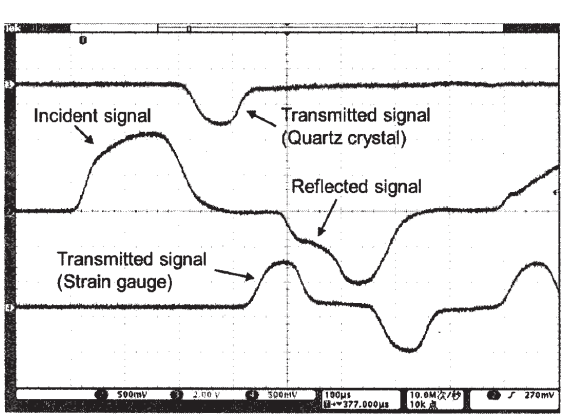


Fig. 2.Oscilloscope signals for a typical test.

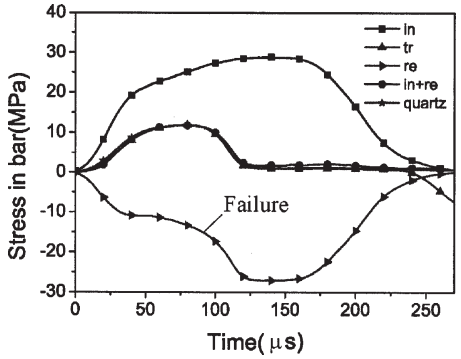


Fig. 3. Dynamic stress equilibrium check of a typical test

or the signal from the quartz crystal directly. It can be seen from figure 3 that, the transmitted stress wave obtained by the strain gauges (Tr) and that obtained from the incident side (In+Re) are just the same. Thus, the hypothesis of dynamic stresses equilibrium is achieved during the loading. When the stress state is uniform throughout the specimen, the result of 1-wave analysis and the 2-wave analysis is the same in this condition, we use the results of 1-wave analysis in our tests. In addition, the stress obtained by the strain gauges (Tr)is the same as that obtained from the quartz crystal (Quartz), whereas the amplitude of the quartz crystal is about four times of the one obtained by the strain gauge.

Figure 4 illustrates the stress-strain curves of the PBX with the strain rates from $1.67\times10^{-5}$ $s^{-1}$ to 500 $s^{-1}$. A nonlinear increase of the stress is observed as the strain increases before the maximum stress point is reached. This is for the reason that local yielding occurs at a much lower stress. It is also found that the PBX exhibit significant viscoelastic effect. The PBX failed at the peak stress, which is denoted as the compression strength. After that, the stress decreased rapidly as the strain increases. The PBX also exhibited significant brittleness. For the test with the strain rate of 60 $s^{-1}$, the sample was not destroyed but simply unloaded until the end of the load. This is because the micro-cracks in the sample did not fully extend to the degree that macroscopic failure required in the low strain rate experiment.

The plastic and brittleness behaviour can be explained by the PBX complex compositions. The energetic crystalline particles of the PBX are brittle. However, the strength of the binder matrix, which plays an important role in the mechanical responses as a plastic material, is very low. The mechanical properties of the PBX are affected by the combined effects of the two materials. Figure 4 indicates that the compressive strength increases with the increasing of load strain rate. Increasing from ~ 35.8MPa at the strain rate of $1.67\times10^{-5}$ $s^{-1}$ to ~ 47.9 MPa at the strain rate of 500 $s^{-1}$, nearly a 33.8% increment in the compressive strength is found. The relationship of the compressive strength and the logarithmic strain rate is shown in figure 5.The error bars were obtained by five tests at each condition. It is found that the compressive strength increased linearly as the logarithmic strain rate increases and it showed a strain rate-enhancement effect.

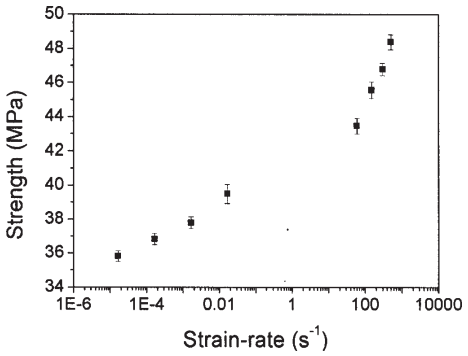


Fig. 5. Variation in the dynamic compressive strength with strain rate

*Fracture tests*

The fracture tests were conducted by the notched semi-circular bend (NSCB) specimen, as shown in figure 6. The fracture toughness is obtained by a MTS machine using the NSCB specimen. The mode-I stress intensity factor history can be calculated as[20]:

$$K_I(t)=\frac{F(t)S}{BR^{3/2}}\cdot Y(\frac{a}{R}) \qquad (6)$$

where $F(t)$ is the load force history, $S$, $B$, $a$, and $R$ are the geometry parameters of NSCB specimen [21], and $Y(a/R)$ a dimensionless geometry factor [22,23].The way to obtain the fracture toughness from the stress intensity factor following the ASTM (American Society of Testing and Materials)standard E1820[24]. The fracture toughness of the PBX is 0.83MPa $m^{1/2}$.

The dynamic fracture parameters are obtained by the newly proposed method –NSCB specimen loaded with SHPB was used in this study[21]. As reported before, equation (6) is valid when the force balance is satisfied during the dynamic test [21]. The pulse shaper technique is used to in the experiment to achieve dynamic force balance on two ends of the specimen [25,26]. The dynamic fracture velocity are measured by the crack propagation gauge mounted on the specimen [27].The experimental results of fracture tests are shown in table 2.

**Visco-SCRAM Model**

Rangaswamy et al. applied the Visco-SCRAM model to simulate the stress–strain response and the three-point

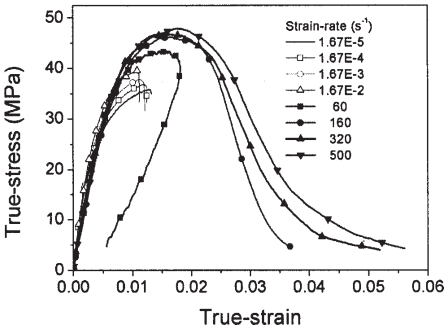


Fig. 4. Dynamic compressive stress–strain curves under different strain rate loading

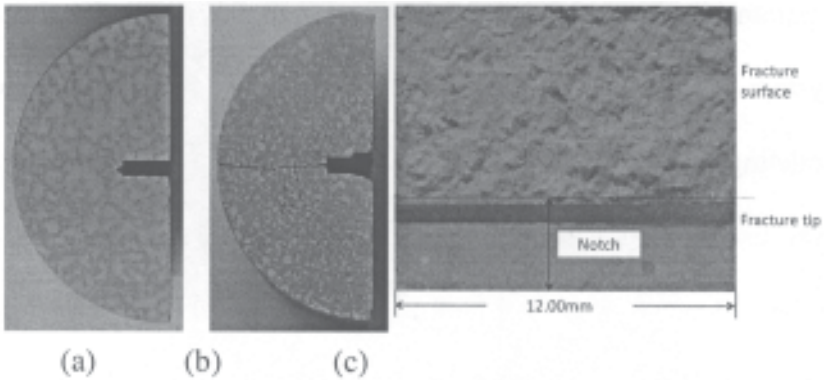


Fig. 6. Photo of the NSCB specimen: (a) before the test, (b) after the test, and (c) the fracture surface.

**Table 2**
EXPERIMENTAL RESULTS OF FRACTURE TESTS

| NO. | $K_{IC}^{d}$/MPa m$^{1/2}$ | $v$/ m s$^{-1}$ |
|---|---|---|
| 1# | 0.948 | 95 |
| 2# | 0.854 | 60 |
| 3# | 0.836 | 75 |
| 4# | 0.855 | 45 |
| 5# | 1.33 | 220 |
| 6# | 1.11 | 170 |
| 7# | 1.90 | 280 |

bending test of PBX9501[2]. In this study, due to the significant plastic effect of the PBX explosives, the Visco-SCRAM model is used. In the Visco-SCRAM model, the stress is decomposed into hydrostatic and deviatoric parts, where $p$ and $s$ indicate the pressure and stress deviator, respectively

$$\sigma_{ij} = S_{ij} + p\delta_{ij} \tag{7}$$

The deviatoric parts are considered to be viscoelastic property, which are used by the generalized deviatoric Maxwell model, and for the individual elements the strain is common while the stresses are added up, i.e., [15]

$$S_{ij} = \sum_{n=1}^{N} (2G^{(n)}\dot{e}_{ij}^{ve} - \frac{s_{ij}^{(n)}}{\tau}) \tag{8}$$

where $N$ is the number of elements in the generalized Maxwell model, $G^{(n)}$, $\tau^{(n)}$ and $s_{ij}^{(n)}$ are the shear modulus, the relaxation time, and the deviatoric stress component of the n$^{th}$ element, respectively. If the loading strain rate is a constant, $\dot{e}_{ij}^{ve}$ is a constant value and $e_{ij}^{ve}=t\dot{e}_{ij}^{ve}$. Considering the initial condition of $s_{ij}^{ve}=0$ MPa and $e_{ij}^{ve}=0$, the solution of eq. (8) is derived as

$$S_{ij}^{ve} = 2G\tau\dot{e}_{ij}^{ve} \cdot [1 - \mathrm{Exp}(-\frac{e_{ij}^{ve}}{\tau\dot{e}_{ij}^{ve}})] \tag{9}$$

The corresponding generalized Maxwell model relationship between the deviatoric stress rate and deviatoric strain rate is

$$S_{ij} = \sum_{n=1}^{N} \left\{ 2G^{(n)}\tau^{(n)}\dot{e}_{ij}^{ve} \cdot \left[ 1 - \mathrm{Exp}(-\frac{e_{ij}^{ve}}{\tau^{(n)}\dot{e}_{ij}^{ve}}) \right] \right\} \tag{10}$$

Under uniaxial loading conditions, the three strain components are ($\varepsilon$, $-\upsilon\varepsilon$, $-\upsilon\varepsilon$), and the three stress components are ($\sigma$, 0, 0). The conversion relationship between the measured stress and strain with the deviatoric stress and strain is

$$\begin{cases} S_{11} = \frac{2}{3}\sigma \\ S_{22} = -\frac{1}{3}\sigma \\ S_{33} = -\frac{1}{3}\sigma \end{cases}, \quad \begin{cases} e_{11} = \frac{2}{3}(1+\nu)\varepsilon \\ e_{22} = -\frac{1}{3}(1+\nu)\varepsilon \\ e_{33} = -\frac{1}{3}(1+\nu)\varepsilon \end{cases} \tag{11}$$

Combining eqs. (10) and (11) yields

$$\sigma = \sum_{n=1}^{N} \left\{ 2G^{(n)}\tau^{(n)}(1+\nu)\dot{\varepsilon} \cdot \left[ 1 - \mathrm{Exp}(-\frac{\varepsilon}{\tau^{(n)}\dot{\varepsilon}}) \right] \right\} \tag{12}$$

Equation (12) is the generalized Maxwell model relationship under constant strain rate uniaxial loading.

The relationship between the cracking deviatoric strain and the deviatoric stress is

$$e_{ij}^{cr} = \frac{c^3}{2Ga^3} S_{ij} \tag{13}$$

where $c$ is the average crack radius and $a$ is the initial flaw size.

It is assumed that the crack growth rate depends on the stress intensity [15]

$$\dot{c} = \frac{v_{\max}}{1+\frac{2}{m}} \left( \frac{K}{K_0\sqrt{1+\frac{2}{m}}} \right)^m \quad K < K_0\sqrt{1+\frac{2}{m}} \tag{14}$$

$$\dot{c} = v_{\max}[1 - (\frac{K_0}{K})^2] \quad K \geq K_0\sqrt{1+\frac{2}{m}} \tag{15}$$

where $K_0$ is the fracture toughness of PBX, $K$ is the stress intensity factor and $K^2 = \pi \cdot c \cdot \sigma_{eff}^2 = \frac{3}{2}\pi \cdot c \cdot S_{ij}S_{ij}$. The parameter $m=10$ is suggested by [15], and $v_{max}$ = 361m/s can be fitted by the data of table 2. The total deviatoric strain can be represented as the sum of the viscoelastic deviatoric strain and the cracking deviatoric strain.

$$e_{ij} = e_{ij}^{ve} + e_{ij}^{cr} \tag{16}$$

The expression of the deviatoric stress rate for the nth Maxwell element is given by [15]

$$\dot{S}_{ij}^{(n)} = 2G^{(n)}\dot{e}_{ij} - \frac{S_{ij}^{(n)}}{\tau^{(n)}} - \frac{G}{G^{(n)}} \left[ 3(\frac{c}{a})^2 \frac{\dot{c}}{a} S_{ij} + (\frac{c}{a})^3 \dot{S}_{ij} \right] \tag{17}$$

**Elastic-Plastic SCRAM Model**

In this section, firstly the generalized deviatoric Maxwell model can be deleted, and the elastic-plastic model including crack is presented. Secondly, the effects of pressure are considered in the damage evolution law.

The total deviatoric strain can be divided into three parts, such as the elastic deviatoric strain, the plastic deviatoric strain and the cracking deviatoric strain, and the relation is given by

$$e_{ij} = e_{ij}^{e} + e_{ij}^{p} + e_{ij}^{cr} \tag{18}$$

As an approximation, over a small time step cracking deviatoric strain and plastic deviatoric strain are independent to each other and calculations can be done separately. That is to say, each step can be divided into two sub-steps calculation. Firstly the cracking deviatoric strain $e_{ij}^{cr}$ is calculated by the crack growth $\Delta c$ and the stress predicted in the first sub-step calculation in which plasticity is not involved. Secondly the plastic response can be added and the final stress of each step can be used to update (correct) the stress predicted in the first sub-step calculation [28].

For simplicity, the plastic response can be represented by the von-Mises theory with rate-independent. The yield surface in the von-Mises theory is given by

$$f(\sigma) = \overline{\sigma} - \sigma_y \tag{19}$$

where $\overline{\sigma}$ is the equivalent (von-Mises) stress, and $\sigma_y$ is the yield stress. In general, the yield stress can be taken as a function of the plastic strain, the strain rate, and the temperature. Also for simplicity, the yield stress $\sigma_y$ is assumed to vary with the strain rate according to Johnson-Cook model. The yield stress $\sigma_y$ is given by

$$\sigma_y = \sigma_{y0}\left(1 + C\ln\frac{\dot{\varepsilon}_p}{\dot{\varepsilon}_0}\right) \quad (20)$$

where $\sigma_{y0}$ is the initial yield stress, $C$ is constant, $\varepsilon_p$ is the effective plastic strain, and $\dot{\varepsilon}_p = 1s^{-1}$.

In the Elastic-Plastic-SCRAM model, the pressure expression was obtained from the porous materials [14]

$$p = wp_s(wv, e) \quad (21)$$

and

$$\dot{p} = -wK\frac{\dot{v}}{v} + [(1+2\Gamma_s)p - wK]\frac{\dot{w}}{w} + \frac{\Gamma_s T\dot{s}}{v} \quad (22)$$

where $w$ is the solidity (the ratio of the specific volume of the solid constituent to the total specific volume), $\Gamma_s$ is Gruneisen constant of the solid material. $s$ and $v$ are the entropy and volume of the solid material, respectively. $T$ is the temperature.

It is assumed that all inelastic strain contributes to internal heating and the contributions to the stored internal energy in the fracture surface are ignored. Therefore, in the absence of thermal conduction, the production of the entropy is entirely due to the inelastic strain. Hence

$$\rho T\dot{s} = s_{ij}\dot{e}^c_{ij} + s_{ij}\dot{e}^p_{ij} - p\dot{\varepsilon}^c_{kk} \quad (23)$$

$$\dot{\varepsilon}^c_{kk} = -\dot{w}/w \quad (24)$$

Thus, the pressure–volume response of the material is expressed as

$$\dot{p} = -wK\dot{\varepsilon}_{kk} + [wB_s - (1+2\Gamma_s)p]\dot{\varepsilon}^c_{kk} + \Gamma_s s_{ij}\dot{e}^c_{ij} + \Gamma_s s_{ij}\dot{e}^p_{ij} \quad (25)$$

## Implementation in Abaqus

Based on the experimental results of the PBX material, the stress $\sigma$ can be obtained at the strain of $\varepsilon_0 = 1.09\%$. Eq. (10) can be fitted with the given stress $\sigma$ and strain rate, and the fitted data are shown in table 3 and table 4. Note that we have five valid tests for each strain rate, so there are 40 samples for the fitting. The value of initial flaw size $a$ is given by the manufacturer[17].The constant $m$ and $c_0$ are following the one of PBX9501[15]. The parameters of micro-cracks $K_0$ and $v_{max}$ are obtained by the fracture test.

The constitutive model formulations [eqs. (16) and (21)] are employed for a user subroutine implemented in the ABAQUS/explicit finite element code. The uniaxial stress-strain relationships are obtained by applying the Visco-SCRAM model and the Elastic-Plastic-SCRAM model in the simulations. The stress-strain curves predicted by both two models for different strain rates are shown in figure7. The trends of the predicted stress–strain responses under different strain rates are found to be similar to that of the experimental results. Under low strain rate conditions, the predicted results of these two models agree well, whereas the simulated results are found to be more brittle than the experimental results. Figure8 shows the stress–strain responses of the PBX predicted by the Visco-SCRAM model and the Elastic-Plastic-SCRAM model at a loading strain rate of 500 $s^{-1}$. It is found that the stress–strain response predicted by the Visco-SCRAM model is relatively more brittle than that predicted by the Elastic-Plastic-SCRAM model. However, the maximum stress predicted by the Visco-SCRAM model is much higher than the experimental results, while good agreement is found between the prediction of the Elastic-Plastic-SCRAM model and the experimental results. Therefore, the Elastic-Plastic-SCRAM model is recommended to simulate the dynamic behaviour under high strain rate conditions.

In the Visco-SCRAM model, the viscoelastic and brittle deformation is mainly considered, and plastic deformation is ignored. The stress-strain results show that the stress increased to the peak which is an over-prediction of the actual stress at relatively low strain. It is shown that the crack grows faster in the Visco-SCRAM model than that in

**Table 3**
DYNAMIC PARAMETERS OF THE PBX IN VISCO-SCRAM MODEL

| Item | Value |
|---|---|
| $G^{(1)}$ (MPa) | 1,250 |
| $G^{(2)}$ (MPa) | 204 |
| $G^{(3)}$ (MPa) | 10.2 |
| $G^{(4)}$ (MPa) | 49.3 |
| $G^{(5)}$ (MPa) | 802 |
| $\tau^{(1)}$ (s) | $\infty$ |
| $\tau^{(2)}$ (s) | 1 |
| $\tau^{(3)}$ (s) | 1.0E-2 |
| $\tau^{(4)}$ (s) | 1.0E-4 |
| $\tau^{(5)}$ (s) | 1.0E-6 |
| $\nu$ | 0.329 |
| $K_0$ (MPa·m$^{1/2}$) | 0.83 |
| $v_{max}$ (m/s) | 361 |
| $m$[15] | 10 |
| $a$ (m)[17] | 1.00 E-3 |
| $c_0$ (m)[15] | 3.00 E-5 |

**Table 4**
DYNAMIC PARAMETERS OF THE PBX IN THE ELASTIC-PLASTIC-SCRAM MODEL

| Item | Value |
|---|---|
| $G$ (MPa) | 1,410 |
| $\nu$ | 0.329 |
| $\sigma_{y0}$ (MPa) | 48 |
| C | 0.017 |
| $\Gamma_s$ | 1.5 |
| $K_0$ ( Pa·m$^{1/2}$ ) | 0.83 |
| $v_{max}$(m/s) | 361 |
| $m$[15] | 10 |
| $a$ (m)[17] | 1.00 E-3 |
| $c_0$ (m)[15] | 3.00 E-5 |

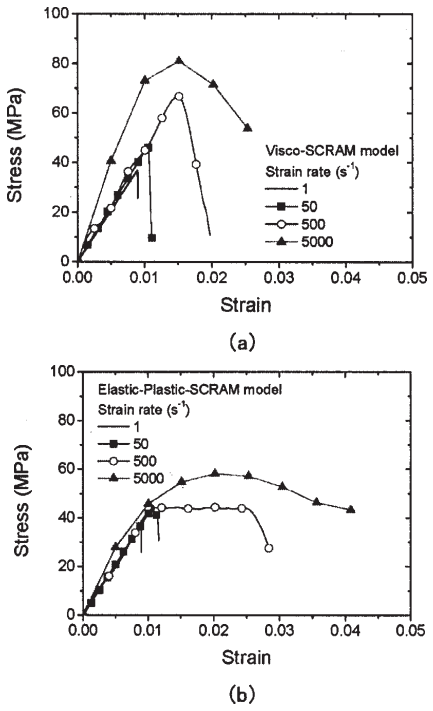


Fig. 7. The stress–strain curves obtained by (a) the Visco-SCRAM model and (b) the Elastic-Plastic-SCRAM model.

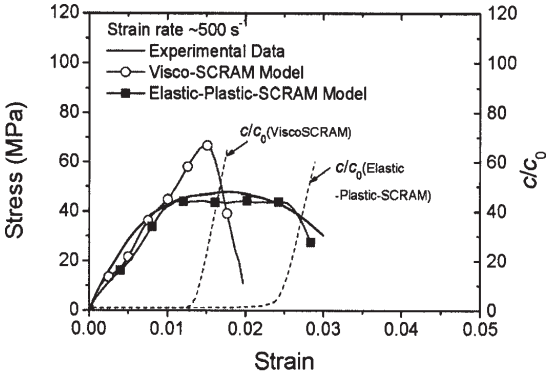


Fig. 8. Comparison of the stress–strain curves between the simulation results and the experimental data. The dash lines are the crack length histories of both models. The crack growth in the Visco-SCRAM model is faster than in the Elastic-Plastic-SCRAM model

the Elastic-Plastic-SCRAM model. Referring to figure 8 the maximum stress reaches 70MPa when strain is 0.015, which in return can lead to a fast growth of the crack and the start of the material large damage. According to the test data, plastic bonded explosives undergo the clear plastic deformation that cannot be neglected in the constitutive relation. In the Elastic-Plastic-SCRAM model, the maximum stress cannot exceed 50MPa, which lead to a relatively slow crack growth, and material begins to soften until the strain is 0.025. For such applications, as in this paper, Elastic-Plastic-SCRAM model can be better justified for the PBX dominated by the plastic and brittle behaviour.

Compared to the constants used in the Visco-SCRAM model, the initial yield stress $\sigma_{y0}$ and the rate-independent constant $C$ need to be obtained beforehand. The current model including both the damage and the plasticity contains less material constants and simple calculations procedure than the Visco-SCRAM model. All in all, the Elastic-Plastic-SCRAM model is more appropriate to quasi-brittle materials which may be dominated by plastic deformation under loading.

## Conclusions

Quasi-static and dynamic experiments on a PBX are conducted, and the stress–strain responses are obtained under different strain rates. Then, the Elastic-Plastic-SCRAM model incorporating the plasticity effects and the equation of state coupled with damage is introduced. FEA simulations are also conducted by applying the Visco-SCRAM model and the Elastic-Plastic-SCRAM model. By comparing the results of the simulations and the tests, it is found that the Elastic-Plastic-SCRAM model better describe the dynamic behaviour of the PBX better for high strain rate loading. Thus, the Elastic-Plastic-SCRAM model can be used for explosive safety applications. In the future, Frictional hot-spots and other Hot-spot models will be further improved by introducing the hot-spot ignition process.

*Acknowledgments: This work was supported by the Open Foundation of State Key Laboratory of Explosion Science and Technology (Beijing Institute of Technology, Grant No. KFJJ11-9Y), and the Natural Science Foundation of China (NSFC) through Grant Nos. 11202232, 11172328&11132012.*

## Notation

$a$ the initial flaw size
$A_0$ the cross-section of the bars
$A_s$ the initial area of the sample
$c$ the average crack radius
$c_0$ the sound speed of the bars
$e_{ij}^{ve}$ the viscoelastic deviatoric strain
$e_{ij}^{cr}$ the cracking deviatoric strain
$e_{ij}$ the total deviatoric strain
$E_0$ the Young's modulus of the bars
$G^{(n)}$ the shear modulus for the n$^{th}$ Maxwell element
$K$ the bulk modulus
$k_0$ the scale factor of the charge amplifier
$k_1$ the scale factor of the pre amplifier
$k_2$ the strain gauge coefficient
$k_{QC}$ the quartz crystal coefficient
$l_0$ the length of the specimen
$p$ the pressure
$S_{ij}$ the stress deviator
$s$ the entropy of the solid material
$\mathring{s}_{ij}^{(n)}$ the deviatoric stress rate for the n$^{th}$ Maxwell element
$U_Q$ the signal of quartz crystal
$v$ the volume of the solid material
$w$ the solidity
$\varepsilon_i(t)$ the incident strain history
$\varepsilon_r(t)$ the reflected strain history
$\varepsilon_t(t)$ transmitted strain history
$\dot{\bar{\varepsilon}}_p$ the effective plastic strain
$\tau^{(n)}$ the relaxation time for the n$^{th}$ Maxwell element
$\Gamma_s$ the Gruneisen constant
$\sigma_y$ the yield stress
$\bar{\sigma}$ the equivalent (von-Mises) stress
$\sigma_{y0}$ the initial yield stress

## References

1.ELBEIH, A.; JUNGOVA, M.; ZEMAN, S.; VAVRA, P.; AKSTEIN, Z., Explosive strength and impact sensitivity of several pbxs based on attractive cyclic nitramines. Propellants, Explos., Pyrotech.2012, 37, 329-334.

2.RANGASWAMY, P.; THOMPSON, D.G.; LIU, C.; LEWIS, M.W. In Modeling the mechanical response of pbx 9501, 14th International Detonation Symposium, Coeur d'Alene, Idaho, 11 -16 April, 2010; Coeur d'Alene, Idaho, pp. 18277.

3.BLUMENTHAL, W.R.; THOMPSON, D.G.; CADY, C.D.; B!, G.T.G.; IDAR, D.J. In Compressive properties of PBXN-110 and its HTPB-based binder as a function of temperature and strain rate, 12th International Detonation Symposium, San Diego, California, 11 - 16 August, 2002; pp. 201-208.

4.RAE, P.J.; GOLDREIN, H.T.; PALMER, S.J.P.; FIELD, J.E. In The use of digital image cross-correlation (DICC) to study the mechanical properties of a polymer bonded explosive (PBX), Proceedings 12th International Detonation Symposium, San Diego, California, 11 - 16 August, 2002; pp. 112-119.

5.RAE, P.J.; GOLDREIN, H.T.; PALMER, S.J.P.; FIELD, J.E.; LEWIS, A.L., Quasi-static studies of the deformation and failure of beta-hmx based polymer bonded explosives. Proc. R. Soc. Lond. A2002, 458, 743-762.

6.DUNCAN, E.J.S.; MARGETSON, J., A nonlinear viscoelastic theory for solid rocket propellants based on a cumulative damage approach. Propellants, Explos., Pyrotech.1998, 23, 94-104.

7.LUO, J.R. PBX's damage, fracture and constitutive relationship. China Academy of Engineering Physics, Mianyang, 2001 (In Chinese).

8.LI, J.L.; LU, F.Y.; QIN, J.G.; CHEN, R.; ZHAO, P.D.; LAN, L.G.; JING, S.M., Effects of temperature and strain rate on the dynamic responses of three polymer-bonded explosives. J. Strain Anal. Eng. Des.2012, 47, 104-112.

9.DIENES, J.K.; ZUO, Q.H.; KERSHNER, J.D., Impact initiation of explosives and propellants via statistical crack mechanics. J. Mech. Phys. Solids 2006, 54, 1237-1275.

10.DIENES, J.K. Statistical crack mechanics; LA-UR-83-1705; Los Alamos National Laboratory: Los Alamos, NM, USA, 1983.

11.ZUO, Q.H.; ADDESSIO, F.L.; DIENES, J.K.; LEWIS, M.W., A rate-dependent damage model for brittle materials based on the dominant crack. Int. J. Solids Struct.2006, 43, 3350-3380.

12.DIENES, J.K., Frictional hot-spots and propellant sensitivity. Proc. Mat. Res. Soc. Symp.1984, 24.
13.ADDESSIO, F.L.; JOHNSON, J.N., A constitutive model for the dynamic response of brittle materials. J. Appl. Phys.1990, 67, 3275-3286.
14.HACKETT, R.M.; BENNETT, J.G., An implicit finit element material model for energetic particulate composite materials. Int. J. Num. Meth. Engng.2000, 49, 1191-1209.
15.BENNETT, J.G.; HABERMAN, K.S.; JOHNSON, J.N.; ASAY, B.W.; HENSON, B.F., A constitutive model for the non-shock ignition and mechanical response of high explosives. J. Mech. Phys. Solids 1998, 46, 2303-2322.
16.KUMAR, A.S.; RAO, V.B.; SINHA, R.K.; RAO, A.S., Evaluation of plastic bonded explosive (pbx) formulations based on rdx, aluminum, and htpb for underwater applications. Propellants, Explos., Pyrotech.2010, 35, 359-364.
17.WEI, J.Z.; YU, K.; LIANG, X.L., Specification for hexogen. In GJB296A-95, China, 1995 (In Chinese).
18.CHEN, R.; DAI, F.; QIN, J.; LU, F., Flattened brazilian disc method for determining the dynamic tensile stress-strain curve of low strength brittle solids. Exp. Mech.2013, 53, 1153-1159.
19.XIA, K.; NASSERI, M.H.B.; MOHANTY, B.; LU, F.; CHEN, R.; LUO, S.N., Effects of microstructures on dynamic compression of barre granite. Int. J. Rock Mech. Min. Sci.2008, 45, 879-887.
20.CHONG, K.P.; KURUPPU, M.D., New specimen for fracture-toughness determination for rock and other materials. Int. J. Fract. 1984, 26, R59-R62.
21.CHEN, R.; XIA, K.; DAI, F.; LU, F.; LUO, S.N., Determination of dynamic fracture parameters using a semi-circular bend technique in split hopkinson pressure bar testing. *Eng. Fract. Mech.*2009, *76*, 1268-1276.
22.DAI, F.; CHEN, R.; XIA, K., A semi-circular bend technique for determining dynamic fracture toughness. Exp. Mech.2010, 50, 783-791.
23.BARSOUM, R.S., Triangular quarter-point elements as elastic and perfectly-plastic crack tip elements. Int. J. Num. Meth. Engng.1977, 11, 85-98.
24. *** Standard test method for measurement of fracture toughness. In ASTM-E1820-08, ASTM International: 2009; Vol. 08, pp 1-48.
25.FREW, D.J.; FORRESTAL, M.J.; CHEN, W., Pulse shaping techniques for testing brittle materials with a split hopkinson pressure bar. Exp. Mech.2002, 42, 93-106.
26.WEERASOORIYA, T.; MOY, P.; CASEM, D.; CHENG, M.; CHEN, W., A four-point bend technique to determine dynamic fracture toughness of ceramics. J. Am. Ceram. Soc.2006, 89, 990-995.
27.JIANG, F.; ROHATGI, A.; VECCHIO, K.S.; ADHARAPURAPU, R.R., Crack length calculation for bend specimens under static and dynamic loading. Eng. Fract. Mech.2004, 71, 1971-1985.
28.ZOU, Q.H., A crack mechanics based model for damage and plasticity of brittle materials under dynamic loading. Int. J. Solids Struct.2010, 47, 2780-2798.

Manuscript received: 28.04.2014